



**Emerging investigator series: Photocatalysis for MBR
 Effluent Post-Treatment: Assessing the Effects of Effluent
 Organic Matter Characteristics**

Journal:	<i>Environmental Science: Water Research & Technology</i>
Manuscript ID	EW-ART-10-2018-000734.R1
Article Type:	Paper
Date Submitted by the Author:	07-Jan-2019
Complete List of Authors:	Maghsoodi, Mostafa; Louisiana State University, Civil and Environmental Engineering Jacquin, Céline; Institut Europeen des Membranes Teychené, Benoit; Institut de Chimie des Milieux et Materiaux de Poitiers Heran, Marc; Institut Europeen des Membranes Tarabara, Volodymyr; Michigan State University, Civil and Environmental Engineering Lesage, Geoffroy; Institut Europeen des Membranes, Snow, Samuel; Louisiana State University, Civil and Environmental Engineering

This work addresses critical challenges to applying photooxidation processes to waters with significant organic matter content. Fractionation and characterization tools were used to better understand the effects of organic matter on these oxidation pathways. The results guide wastewater reuse efforts by identifying critical impediments to photooxidation processes in wastewater and demonstrating the potential use of membranes to overcome the challenges.

1 **Emerging investigator series: Photocatalysis for MBR Effluent Post-Treatment: Assessing the**
2 **Effects of Effluent Organic Matter Characteristics**

3 Authors:

4 Mostafa Maghsoodi^{1†}, Céline Jacquin^{2†}, Benoit Teychené³, Marc Heran², Volodymyr V.

5 Tarabara⁴, Geoffroy Lesage^{*2}, Samuel D. Snow^{*1}

6 ¹Department of Civil and Environmental Engineering, Louisiana State University, 3255

7 Patrick Taylor Hall, Baton Rouge, Louisiana 70803, United States.

8 ²IEM (Institut Européen des Membranes), UMR 5635 (CNRS-ENSCM-UM),

9 Université de Montpellier, Place E. Bataillon, F- 34095, Montpellier, France.

10 ³Institut de Chimie des Milieux et Matériaux de Poitiers (IC2MP – UMR CNRS 7285),

11 Université de Poitiers, Ecole Nationale Supérieure d'Ingénieurs de Poitiers, 7 rue Marcel

12 Doré, Bâtiment 16, TSA 41105, 86073 Poitiers Cedex 9, France.

13 ⁴Department of Civil and Environmental Engineering, Michigan State University, 428 S. Shaw

14 Lane, East Lansing, Michigan 48824, United States.

15 [†]These authors contributed equally.

16 *Corresponding authors: SSnow@lsu.edu; Geoffroy.Lesage@umontpellier.fr;

17

18 **Abstract:** Dissolved organic matter (DOM) poses a serious challenge to applied photocatalysis.

19 Membranes may offer a promising synergistic opportunity to enable efficient photocatalysts in

20 the presence of DOM. Membrane bioreactor (MBR) effluent from a municipal treatment plant
21 was studied to elucidate the effects of filtration and organic matter composition on
22 photocatalysis. Effluent samples were collected from MBR units during routine operation and
23 before/after chemical cleaning. Additional DOM samples from the bulk supernatant were
24 separated into colloidal, hydrophobic and transphilic fractions, providing a novel examination
25 of the inhibition potential of DOM. These DOM fractions and the effluent organic matter (EfOM)
26 samples were then characterized utilizing three-dimensional excitation–emission matrix
27 (3DEEM) fluorescence spectroscopy and assayed for their potential to inhibit TiO₂-mediated
28 photocatalytic degradation of a probe compound, *para*-chlorobenzoic acid (*p*CBA). The
29 colloidal fraction of DOM was found to exert the strongest inhibition, followed by the transphilic,
30 then the hydrophobic fractions; at 5 mgC/L, these fractions reduced the photodegradation rates
31 by approximately 75%, 27%, and 17%, respectively. Of the effluent samples, EfOM from the
32 recently-cleaned membrane caused the greatest inhibition of photocatalysis (~100% reduction
33 at 0.5 to 2.0 mgC/L), whereas the effluent from the fouled membrane provided the least
34 inhibition (~33% reduction at 2.0 mgC/L). The 3DEEM analysis predicted inhibitory action of
35 both DOM and EfOM, based on total fluorescence volumes. Results here demonstrate the
36 prospective utility of combining membrane technologies with photocatalytic processes.

37

38 1. Introduction

39 As the human population continues to grow, careful utilization of natural resources becomes
40 increasingly more important. Water usage, and particularly reuse, is a critical topic for many
41 communities.^{1, 2} The development of membrane bioreactor (MBR) technology has been an
42 important step towards wastewater reuse, given substantial advantages over conventional
43 activated sludge systems in terms of improved efficiency and effluent quality.³ Despite these
44 benefits that stem from the use a physical barrier (membranes), several types of contaminants
45 can pass through the membranes and pose significant health risks upon release of the effluent
46 into the environment. Indeed, viruses have been found in the effluents of state-of-the-art MBR
47 treatment plants.^{4, 5} In addition, pharmaceuticals^{6, 7} and, more recently, antibiotic resistant
48 genes have drawn attention as significant concerns posing environmental and health risks.⁸
49 Thus, MBR systems require a disinfection step post-filtration to provide a safeguard. Although
50 UV disinfection can be used in lieu of chlorination, and thereby avoid the necessity for an
51 added dechlorination step, there are disadvantages: UV treatment does not significantly
52 degrade antibiotic resistant genes⁸ and many pollutants are recalcitrant to UV at commonly
53 applied UV doses.⁹
54 Given these post-filtration challenges, an integration of innovative technologies could provide
55 the key functionality to eliminate the remaining hazards from MBR effluent. In particular,

56 photocatalytic materials applied in conjunction with existing UV dosing systems could produce
57 reactive oxygen to destroy these contaminants via advanced oxidation processes.⁹⁻¹²
58 Germicidal UV radiation, a subset of the spectrum of short-wavelength UV light, often called
59 UVC,^{13, 14} can be enhanced by the addition of photocatalytic processes to promote the
60 production of reactive oxygen species (ROS). These ROS are known to be particularly effective
61 at inactivating viruses compared to bacteria which have protective cell membranes.¹⁵⁻¹⁸ For
62 example, the inactivation kinetics *Escherichia coli* by hydroxyl radicals ($\cdot\text{OH}$) or by singlet
63 oxygen ($^1\text{O}_2$) have been shown to have a lag-phase where the cell membrane protects the
64 bacteria's intracellular components against ROS attack,^{15, 16, 18} whereas the genetic and
65 essential components of viruses, such as MS2 bacteriophage, have very little protection and
66 therefore no delay in their inactivation kinetics.^{15, 16} A combined UVC-photocatalytic system is
67 a plausible conception that could serve as an advanced oxidation process to oxidize
68 pharmaceutical compounds in addition to providing disinfection activity.¹⁰

69 Application of photocatalytic processes to natural or waste waters faces a significant challenge
70 in the form of non-target organic matter interferences. In the case of MBRs, effluent organic
71 matter (EfOM) contains a variety of molecules that are known to quench hydroxyl radicals
72 ($\cdot\text{OH}$),¹⁹ which are generally the most important ROS in any advanced oxidation—including
73 TiO_2 mediated photocatalysis. MBR EfOM is a complex mixture of organic molecules such as

74 proteins, polysaccharides, humic substances and nucleic acids.²⁰⁻²³ These molecules originate
75 primarily from microbial activity (soluble microbial products, SMPs), produced during
76 secondary biological treatment (via suspended or attached growth processes) , and are
77 typically found at concentrations ranging from 3 to 25 mgC/L.^{21, 22, 24-27} EfOM can interfere with
78 photocatalytic treatment through different inhibitory mechanisms. First, EfOM absorbs
79 significant amounts of UV light, limiting the amount of photons available for catalyst
80 excitation.²⁸ Second, EfOM quenches ROS, preventing reactions with the target compounds
81 or microorganisms.^{29, 30} This competition for ROS between the non-target EfOM and the target
82 constituents can occur in two ways: scavenging of surface-bound ROS by EfOM and
83 quenching of bulk phase ROS.^{15, 29, 31, 32} Within the complex mixture of EfOM, less than 2% of
84 the dissolved and colloidal organic materials are considered target contaminants, such as
85 viruses or pharmaceuticals that originate from the influent wastewater;³³ thus, most
86 photocatalytically generated $\cdot\text{OH}$ radicals will be quenched by reactions with non-target EfOM.
87 Indeed, EfOM has been reported to scavenge between 65 and 95% of $\cdot\text{OH}$ in conventional
88 effluents and is considered the most important $\cdot\text{OH}$ -scavenger in such systems.^{34, 35} EfOM
89 constituents, such as fulvic acid and humic acid (HA), have a net negative charge above pH 3
90 due to the presence of phenolic and carboxylic groups.^{36, 37} These molecules can therefore

91 interact favorably with and adsorb onto the polar surface of TiO_2 , reacting directly with ROS
92 production sites.

93 It is important to understand the factors that control surface and bulk quenching mechanisms;
94 ROS-EfOM reactivity and EfOM-photocatalyst adsorption affinities drive bulk and surface
95 quenching routes, respectively. Different ROS have differential reactivities; for example, singlet
96 oxygen ($^1\text{O}_2$) is less reactive and more selective than $\cdot\text{OH}$.³⁸ Likewise, EfOM constituents may
97 also vary in propensity to react with ROS, with some compounds being recalcitrant to strong
98 oxidants, while others readily react with weaker ROS, such as $^1\text{O}_2$.^{30, 39} With regard to
99 adsorption interactions, the nature of the photocatalyst surface will determine the type of EfOM
100 molecules that will adsorb onto the photocatalyst surface. These types of interactions have
101 been studied in depth for the case of membrane fouling by organic matter,⁴⁰⁻⁴² and offer
102 potential insights into DOM-photocatalyst interactions.

103 Membrane technology can be used to selectively remove fractions of organic matter. In the
104 case of an MBR treating municipal wastewater, the membrane's material, pore size, and
105 fouling state affect its selectivity and, therefore, the composition of the EfOM.⁴³ It is known that,
106 in general, hydrophilic macromolecular and colloidal portions of organic matter cause more
107 reversible membrane fouling than other fractions in MBR systems by forming a cake layer.⁴¹
108 ^{44, 45} Fouling changes the effective pore size and surface characteristics of membranes;

109 consequently, permeate quality changes over the operational timeline, since the last chemical
110 cleaning event.⁴⁶⁻⁴⁸ Membrane operation may control DOM retention and thereby the
111 composition of DOM that passes through (EfOM); therefore, the time since last cleaning event
112 could be an important parameter when considering the use of effluent disinfection strategies.
113 The extent to which membrane operation time can be used as a control EfOM quality is not
114 well known. A better understanding of the variability of EfOM constituents as a function of
115 membrane operational parameters is critical for applying post-filtration disinfection
116 technologies. Elucidating the effects of membrane operation on EfOM content provides an
117 excellent opportunity to scrutinize the effects of EfOM constituents on photocatalytic
118 processes, a significant area of need for the field of photocatalytic water treatment.

119 While TiO₂ systems have been studied extensively, the mechanisms driving ROS inhibition by
120 DOM are poorly understood. A recent literature review quantified the number of research
121 articles investigating “photocatalysis” and “natural organic matter” and found that of the 17,500
122 papers found when searching for photocatalysis, only 0.8% (137) also referenced DOM.⁴⁹ The
123 segregation of DOM into fractions to discern phenomenological effects of constituents on
124 photocatalytic processes is therefore a critical step towards practical application of
125 photocatalysts. A study completed in 2014 on the effects of size-fractionation of DOM on the
126 photocatalytic degradation of DOM by TiO₂ is perhaps the first report to scrutinize the inhibitory

127 mechanism by analyzing fractionated DOM samples.⁵⁰ The approach in the present study
128 utilizes EfOM from differentially fouled bioreactor membranes and functionally fractionated
129 bioreactor DOM to provide a novel assessment of inhibitory mechanisms of DOM in TiO₂
130 photocatalysis.

131 Bulk supernatant DOM and EfOM samples collected in 2015 and 2016 from an operational
132 MBR in a municipal wastewater treatment plant (WWTP) are studied here. Fractionation of
133 samples in terms of DOM size and hydrophobicity, a method commonly used to isolate
134 organics, was applied to MBR bulk supernatant. Here, the effects of different fractions of bulk
135 supernatant DOM and EfOM samples on photocatalytic processes are assessed to identify the
136 most important fractions to reject during filtration. Three-dimensional fluorescence excitation-
137 emission matrix (3DEEM) analysis is employed to characterize the resultant DOM from
138 fractionation procedures and the MBR effluent samples, to better forecast and understand their
139 effect on photocatalysis processes. 3DEEM is increasingly employed to understand DOM evolution
140 in wastewater systems.^{51, 52} A recent study also highlighted that 3DEEM can be used to distinguish
141 proteins from biopolymers and humic substances and to quantify building blocks, with potential use as
142 an on-line indicator to describe DOM fate and behavior.⁵³ Further, this technique has distinguished
143 the effects of different types of DOM on water treatment technologies (i.e., membrane fouling,
144 UV attenuation, and disinfection byproduct formation).^{43, 54-56} Inhibitory profiles of the DOM
145 fractions and EfOM samples are established by measuring the photodegradation of a

146 molecular probe as a function of total organic carbon (TOC) concentration. Inhibition
147 mechanisms are discussed in the context of an experimentally validated model that accounts
148 for surface and bulk phase quenching processes simultaneously.²⁹ Finally, comments are
149 made on the prospective utility of photocatalytic membrane reactors (PMRs)⁵⁷⁻⁵⁹ as a combined
150 treatment process.

151

152 **2. Materials and methods**

153

154 **2.1. Chemicals**

155 Humic acid and 4-chlorobenzoic acid were obtained from Alfa Aesar (Haverhill, MA). Titanium
156 dioxide (99.9% Anatase) was purchased from Alfa Aesar with a nominal particle size of 32 nm
157 and surface area of 45 m²/g. Ultrapure water (>18.2 MΩ-cm) was produced using a Nanopure
158 Infinity system (Thermo Fisher Scientific Inc., Waltham, MA). HPLC solvents were HPLC-grade
159 and obtained from Alfa Aesar.

160 **2.2. EfOM sampling**

161 EfOM samples were collected from a full-scale MBR wastewater treatment plant (La Grande
162 Motte, France), which treats municipal wastewater and serves a population of approximately
163 60,000. The plant performs biological removal of nitrogen (nitrification and denitrification) and
164 phosphorus. The plant comprises four MBR tanks, each equipped with KUBOTA Submerged

165 Membrane Units® (SMUs, KUBOTA, Japan), which are flat sheet microporous membranes
166 made of chlorinated polyethylene with an average pore size of 0.2 μm and a nominal pore size
167 of 0.4 μm . Only two MBR tanks were studied. Here we define MBR1 as the unit which
168 underwent chemical cleaning and MBR2 as a reference unit that did not undergo chemical
169 cleaning during the sampling period. MBR2 was two months into a three- to four-month cycle
170 and therefore was chosen to represent a membrane during normal operation. To assess the
171 cleaning effect, activated sludge (AS) and permeate samples were taken from MBR1 and
172 MBR2 one day before and one day after the cleaning procedure took place for MBR1 (June
173 2016). After sampling, AS samples were filtered with a 1.2 μm glass microfiber filters (Whatman
174 GF/C) to collect the dissolved portion of the AS, labeled as the bulk supernatant (BSN). Hence,
175 four samples from the MBR1 cleaning campaign and two samples from MBR2 were collected
176 and analyzed for this study: and each sample was given a reference name as shown in Table
177 1.

178 In addition to the samples taken to assess the effects of membrane cleaning, 500 L of AS were
179 also collected from MBR1 in June 2015 to perform DOM fractionation using dialysis and XAD-
180 resins. Prior to fractionation the AS was filtered successively through 50 μm and 2 μm
181 polypropylene filters to collect BSN. Next, softening was performed using a sodium cation-
182 exchange resin (Purolite, France) to remove calcium and magnesium ions, to avoid ion

183 complexation with DOM and scaling during the following step: reverse osmosis (RO).⁶⁰ DOM
184 in the BSN sample was concentrated via RO in order to minimize the time required for the
185 fractionation step. A Filmtec TW 30 membrane was used for the RO process, since it is known
186 to be more resistant to DOM adsorption.⁶¹ The RO process effectively concentrated the BSN
187 by 100-fold which was subsequently used to perform DOM fractionation.

188 2.3. DOM fractionation

189 The first fractionation step consisted of isolating the colloidal portion of DOM by size exclusion,
190 using dialysis (3.5 kDa, Spectra/Por 6 Dialysis Membrane) against HCl (0.01 mol/L, pH 2).
191 Next, organic colloids were separated from colloidal silica and precipitated salts by dialysis
192 (3.5 kDa) against 0.2 mol/L HF.⁶² The dialysate, approximately 30 L of HCl solution containing
193 DOM compounds with a molecular weight smaller than 3.5 kDa, was then passed through
194 XAD8 and XAD4 resins (Amberlite, Sigma Aldrich) arranged in tandem. This step allowed for
195 the collection of hydrophobic (HPO) and transphilic (TPI) fractions.^{42, 63} The hydrophilic (HPI)
196 fraction, composed of low molecular weight hydrophilic DOM and salts, was collected in the
197 outlet of the resins tandem. This fraction, however, was not used in the study because the
198 solution contained highly concentrated salts, which co-precipitate with the organic matter.
199 Removing these salts, while possible, would have required a complex purification step called
200 azeotropic distillation.⁶⁴ To collect HPO and TPI fractions adsorbed onto XAD resins, elution

201 with an acetonitrile/MQ water solution (75/25% v/v) was performed, followed by evaporation
 202 and freeze-drying of the respective organic matter samples.

203

204 Table 1. Nomenclature of samples and fractions based on their respective MBR units, sampling
 205 period, or fractionation procedure.

Label	Collection	Description
BSNf-MBR1	MBR1, Bulk Supernatant	Fouled membrane (Pre-wash)
BSNw-MBR1	MBR1, Bulk Supernatant	Washed membrane (Post-wash)
BSN-MBR2	MBR2, Bulk Supernatant	Midpoint between chemical cleaning events
Pf-MBR1	MBR1, Permeate	Fouled membrane (Pre-wash)
Pw-MBR1	MBR1, Permeate	Washed membrane (Post-wash)
P-MBR2	MBR2, Permeate	Midpoint between chemical cleaning events
C	MBR1, Bulk Supernatant	Colloidal fraction
HPO	MBR1, Bulk Supernatant	Hydrophobic fraction
TPI	MBR1, Bulk Supernatant	Transphilic fraction

206

207 2.4.DOM characterization

208 2.4.1 TOC and UV₂₅₄ absorbance measurements

209 TOC analysis was performed using a TOC-VCSH Shimadzu analyzer (Shimadzu Japan). The

210 UV₂₅₄ absorbance was measured in a 1 cm quartz cuvette using a UV-VIS spectrophotometer

211 (UV-2401PC, Shimadzu, Japan). The specific UV absorbance (SUVA₂₅₄) was then calculated

212 as the ratio of UV₂₅₄ absorbance and TOC value.⁶⁵ These analyses are reported in Table S1.

213 2.4.2. 3DEEM analysis

214 Fluorescence spectra were obtained using a Perkin-Elmer LS-55 spectrometer (USA) and a

215 procedure described elsewhere.⁵³ Spectra were divided into five regions as defined by Chen

216 et al.,⁵⁴ corresponding to different groups of fluorophores. The regions were categorized by
 217 excitation-emission ranges, as noted in Table 2. Region I is associated with aromatic protein-
 218 like fluorophores type I (tyrosine type); Region II is associated to aromatic protein-like
 219 fluorophores type II (tyrosine type); Region III corresponds to fulvic acid-like fluorophores; and
 220 Region IV and V are associated with SMP-like fluorophores (tryptophane type) and humic acid-
 221 like fluorophores, respectively.

222 Table 2. Excitation and emission wavelength classifications of fluorophores.

	Region I	Region II	Region III	Region IV	Region V
Excitation, nm	200 – 250			250 – 350	250 – 500
Emission, nm	280 – 330	300 – 350	380 – 600	280 – 380	380 – 600

223

224 For qualitative analysis, spectra are represented in A.U. (Arbitrary Unit) and rejected fraction
 225 spectra (R) were calculated by subtracting permeate spectra from the BSN spectra, in order
 226 to better visualize the constituents that are rejected by the membrane. For semi-quantitative
 227 analysis, the volume of fluorescence $\Phi(i)$ (Raman Unit.nm²) normalized by the Raman
 228 spectra,⁶⁶ consisting of the integration of the spectral regions, was calculated in the different
 229 spectral regions using the following equation taken from the fluorescence regional integration
 230 (FRI)⁵⁴ method:

$$\Phi(i) = MF(i) \sum_{ex} \sum_{em} I(\lambda_{ex}\lambda_{em}) \Delta\lambda_{ex} \Delta\lambda_{em} \quad (\text{Eq. 1})$$

231

232 where $MF(i)$ is a multiplication factor, $\Delta\lambda_{ex}$ is the excitation wavelength interval (2 nm), $\Delta\lambda_{em}$ is
233 the emission wavelength interval (0.5 nm) and $I(\lambda_{ex}\lambda_{em})$ is the fluorescence intensity at each
234 excitation-emission pair (Raman units). $\Phi(i)$ normalization was necessary to compare values
235 from different regions of the 3DEEM response. To do so, $MF(i)$ was calculated using Equation
236 2.

$$237 \quad MF(i) = \frac{\text{Total spectra area}}{\text{Specific region area}(i)} \quad (\text{Eq. 2})$$

238 For percentage analysis, the ratio between the volume of fluorescence of each region and the
239 total volume was used.

240 2.5. Photochemical experiments

241 Photochemical experiments were conducted in an enclosed UV cabinet with a magnetically
242 stirred photoreactor at room temperature. A 15 W low pressure mercury lamp (Sankyo Denki
243 Co.,) was used as a UVC light source. The distance between the light source and reaction
244 vessel was 20 cm. The irradiance at 254 nm at the location of the vessel was measured to be
245 295 $\mu\text{W}/\text{cm}^2$ with a BLUE-Wave UVNb-25 Spectrometer (StellarNet Inc., Tampa, FL). The
246 UV/Vis emission spectrum for the lamp, shown in Figure S1, was also recorded. The DOM
247 fractions and EfOM samples described above, along with HA, were used to show the inhibitory
248 effect of organic matter on photocatalytic degradation of target pollutants. Experiments utilized

249 15 ml of solution, containing 5 $\mu\text{g/L}$ TiO_2 with 10 μM para-chlorobenzoic acid (ρCBA) as a
250 probe compound that has a known reaction rate constant with $\bullet\text{OH}$.³⁰ HA, DOM fractions, or
251 EfOM samples in various concentrations were added to the reaction solutions to assess the
252 quenching potential of each fraction. Sample aliquots of 0.5 mL were taken at fixed time points
253 and analyzed for ρCBA concentration via HPLC, according to methods reported elsewhere.⁶⁷
254 Briefly, this analysis was conducted with an Agilent HPLC (Agilent technology, 1260 infinity)
255 using a C18 (125 mm) column using acetonitrile and 10 mM phosphoric acid as mobile phase
256 solvents (60:40). The flow rate was 0.5 mL/min and the detection wavelength was 234 nm. For
257 all photochemical reactions, ρCBA degradation rates were obtained by linear regression of
258 plots of ρCBA concentration versus radiant fluence ($\mu\text{J}/\text{cm}^2$). Fluence values were calculated
259 according to Bolton and Linden (2003),⁶⁸ as described previously.⁵⁷ Importantly, these
260 calculations account for reductions in UV_{254} transmission by using sample-specific UV_{254}
261 absorbance values and the transmission distance inside the reactor. The resulting observed
262 photodegradation rates (k_{obs}) were, to a good approximation, first order with respect to radiant
263 exposure (H , $\mu\text{J}/\text{cm}^2$) such that the units of k_{obs} are reported as ($\text{cm}^2/\mu\text{J}$), according to
264 equations (3-6):

$$265 \quad \frac{dC}{dt} = k'_{\text{obs}}C, \quad (\text{Eq. 3})$$

$$266 \quad \frac{1}{H(\mu\text{J}/\text{cm}^2)} \frac{dC}{dt} = \frac{1}{H(\mu\text{J}/\text{cm}^2)} k'_{\text{obs}} C, \quad (\text{Eq. 4})$$

$$267 \quad \frac{dC}{dH} = k_{obs}C, \quad (Eq. 5)$$

268 and

$$269 \quad k_{obs} \left(\frac{cm^2}{\mu J} \right) = \frac{k'_{obs} \left(\frac{1}{s} \right)}{E \left(\frac{\mu W}{cm^2} \right)}. \quad (Eq. 6)$$

270 Here, k'_{obs} (s^{-1}) is the first-order degradation rate constant of p CBA, C is the molar
271 concentration of p CBA, and E is the irradiance ($\mu W/cm^2$) at 254 nm. The differences in the k_{obs}
272 in the presence or absence of organic compounds were used to quantify the inhibitory effect
273 of these compounds. Control experiments were also conducted in the absence of organic
274 matter, TiO_2 , or light.

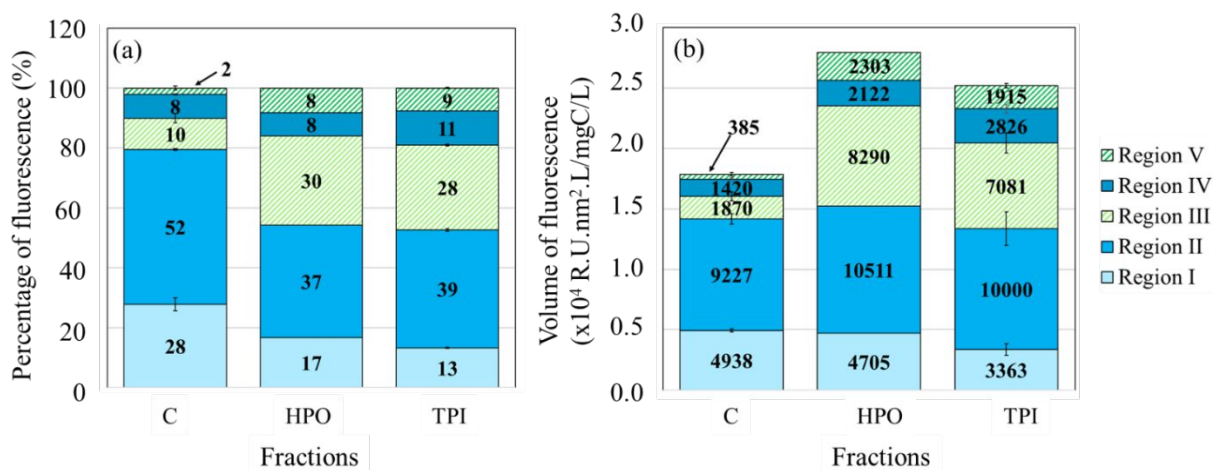
275

276 3. Results

277 3.1. Isolated DOM fractions

278 Prior to performing photocatalytic experiments, DOM fractions were characterized using
279 3DEEM to identify molecular characteristics of DOM within each fraction. The 3DEEM spectra
280 compiled for the fractions are available elsewhere²³ and were used here to quantify the volume
281 of fluorescence and the percentage of fluorescence of each region in Figure 1.

282



283

284 Figure 1. (a) Percentage of fluorescence and (b) Volume of fluorescence of the colloidal (C), HPO and
 285 TPI fractions prepared at 1 mgC/L. Region I, Region II, Region III, Region IV and Region V correspond
 286 to aromatic proteins-like type I, aromatic proteins-like type II, fulvic-like, SMP-like and humic-like
 287 fluorophores, respectively.

288

289 3DEEM analysis showed that each of the three DOM fractions contained both classes of

290 fluorescent compounds: proteins (Regions I, II and IV) and humic substances (Region III and

291 V). However, as seen in Figure 1a, DOM fractions exhibited different fluorescent properties,

292 reflecting differences in their compositions. The percentages of fluorescence of HPO and TPI

293 fractions were similar for all regions and had a dominant proportion of aromatic protein-like

294 type II and fulvic-like fluorophores (Figure 1a). That HPO and TPI compositions did not vary

295 significantly in terms of fluorophore content expected; a study on EfOM of wastewater

296 treatment plants also found that these fractions were similar in terms of fluorophore

297 composition.⁶⁹ For the colloidal fraction, 80% of the fluorescent compounds were aromatic

298 protein-like type I and II fluorophores. Recent studies showed that both protein-like and humic-

299 like fluorophores impact photocatalytic performance. Protein-like constituents were found to
300 react with $\bullet\text{OH}$ radicals in bulk solution,⁵⁵ with reported reaction rate constants of amino acids,
301 proteins, and peptides with $\bullet\text{OH}$ ranging from 1.7×10^7 to 1.05×10^{10} $\text{M}^{-1} \text{s}^{-1}$ (the rate constant
302 between ρCBA and $\bullet\text{OH}$ is similar at 5.2×10^9 $\text{M}^{-1} \text{s}^{-1}$),⁷⁰⁻⁷² while humic-like compounds, having
303 a large number of carboxylic groups, adsorbed onto TiO_2 surfaces, particularly at low pHs.⁷³
304 Thus, the high proportion of fluorescing compounds in Region I and II in colloids, suggests that
305 the colloids may be more reactive with $\bullet\text{OH}$ than HPO and TPI. On the contrary, HPO and TPI
306 are expected to exhibit more surface-phase quenching by adsorbing more strongly onto TiO_2
307 and than the colloids.

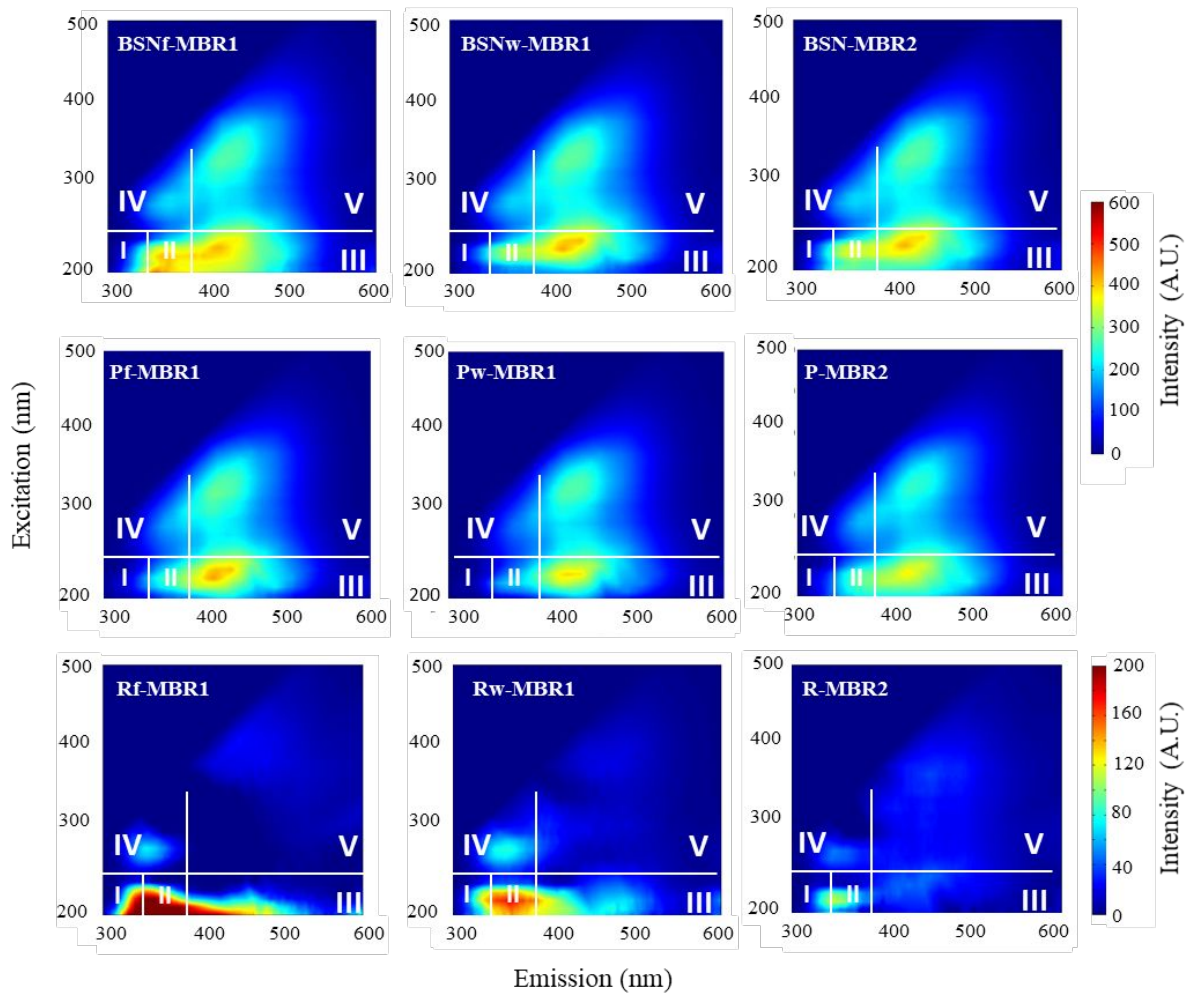
308 The volume of fluorescence is an indicator proportional to the concentration of fluorophores
309 contained in each region. The higher electron density of fluorophores compared with other
310 moieties could yield higher reactivity with ROS, and it would follow, then, that the higher the
311 volume of fluorescence, the higher the quenching of photocatalysis. Thus, from Figure 2b, and
312 hypothesizing that surface-phase quenching is the most problematic for photocatalysis, the
313 DOM quenching potency could be expected in the following order: $\text{HPO} > \text{TPI} > \text{C}$. A similar
314 analysis can be conducted by measuring the SUVA_{254} values as a representation of average
315 aromatic moiety content, which is known to loosely indicate DOM hydrophilicity.⁷⁴ In general,
316 DOM compounds with higher SUVA_{254} values are considered to be more hydrophobic than

317 those with lower values.⁷⁵ In addition, higher $SUVA_{254}$ values correspond to more aromaticity,
318 which could indicate higher reactivity with ROS, given the electron rich moieties. The $SUVA_{254}$
319 values for the colloidal, HPO, and TPI fractions were measured to be 1.8, 2.2, and 1.6 $L \cdot mg^{-1} \cdot m^{-1}$,
320 respectively. Based on this method of analysis, and assuming that electron-dense
321 functional groups are the primary factor in determining ROS quenching, the inhibition capacity
322 of the fractions could be expected in this order: HPO>C>TPI. Neither of these methods are
323 expected to conclusively predict the true inhibition potential, given the many additional factors
324 involved with quenching mechanisms.

325 3.2. EfOM composition and effect of membrane fouling

326 To estimate the effect of membrane fouling and cleaning on the retention of fluorophores,
327 3DEEM spectra of MBR bulk supernatant and permeate were compared (Figure 2). The
328 membranes rejected most compounds from Regions I and II in the three MBR cases studied.
329 This selectivity was apparent in the 3DEEM spectra obtained by subtracting the permeate
330 spectrum from the BSN spectrum. It is likely that most of these aromatic-like fluorophores were
331 associated with organic colloids since they represented 80% of the overall colloidal
332 content. This observation is consistent with a previous study that demonstrated that colloids
333 were major membrane foulants.²³

334



335

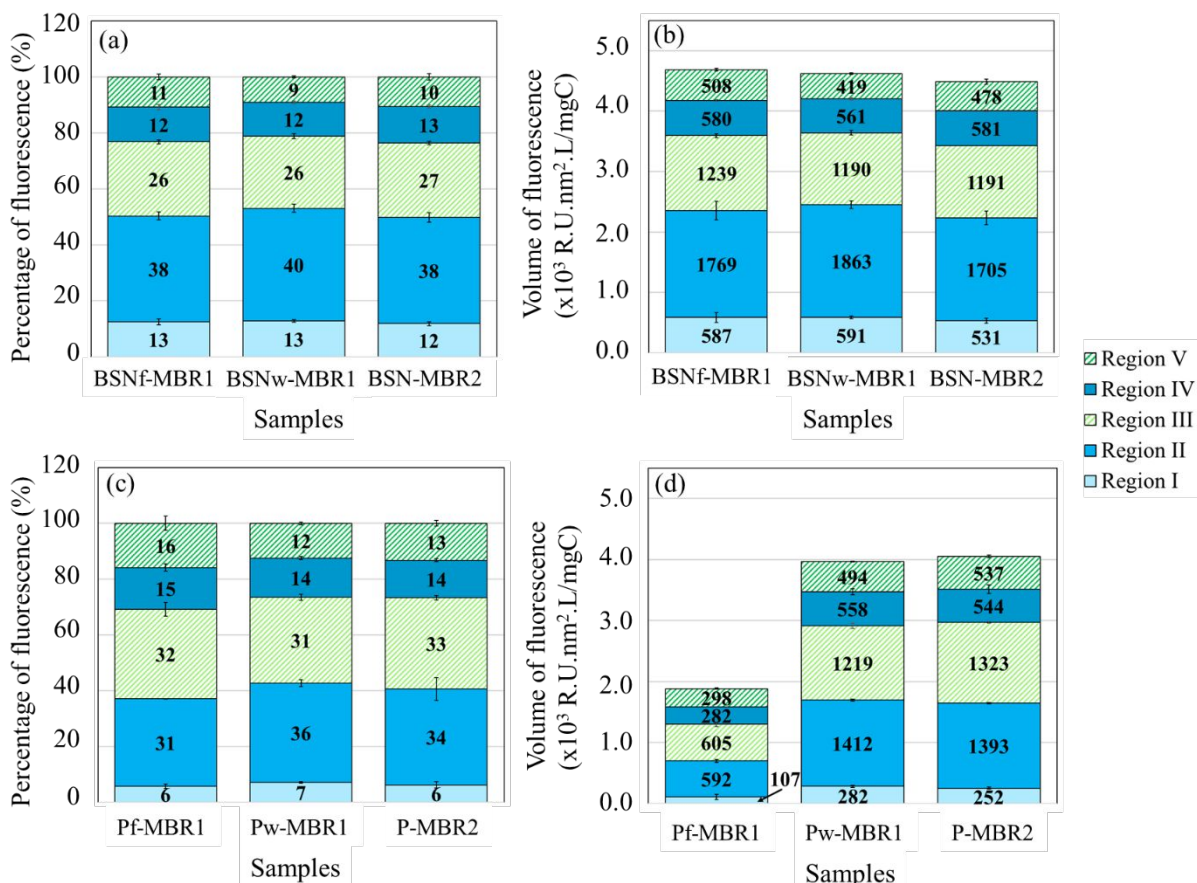
336 Figure 2. Fluorescence spectra of DOM from BSN and EfOM from permeate samples, with I, II, III, IV,
 337 V corresponding to Region I (aromatic proteins-like type I), Region II (aromatic proteins-like type II),
 338 Region III (fulvic-like), Region IV (SMP-like) and Region V (humic-like). R spectra correspond to the
 339 mathematical subtraction of the permeate spectra from the bulk supernatant spectra allowing the
 340 identification of compounds retained by the membrane. Note the different color scale for the R spectra.

341

342

343

344



345
 346 Figure 3. Percentage (a, c) and volume (b, d) fluorescence values for bulk supernatant (a, b) and permeate
 347 (c, d) samples.

348
 349 Figures 3a and 3c show the fluorophore compositions in EfOM samples as percentages of the
 350 different regions; these data showed a preferential rejection of the fluorophores from Region I
 351 and Region II. Indeed, for the three samples, the membrane reduced the fluorescence by 11
 352 ± 2 % in both Region I and II. This reduction corresponded to an increase of fluorescence
 353 percentage of the Regions III and V in the permeate. The relative increase of the humic
 354 substance-related fluorophores confirmed that the membrane preferentially retains colloids,
 355 since they are typically high molecular weight molecules associated with protein-like
 356 fluorophores (Figure 1a).⁵³ Membrane fouling clearly affected the type of fluorophores retained

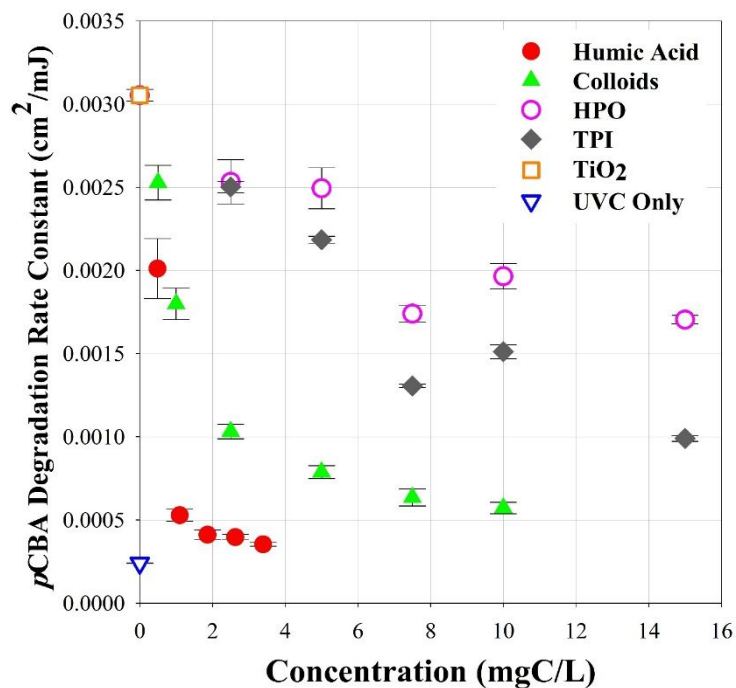
357 in the MBR (Figure 3b and Figure 3d). The three fouling stages present similar bulk
358 supernatant volumes of fluorescence (Figure 3b) and permeate percentage of fluorescence
359 profiles (Figure 3c), but different volumes of fluorescence in the permeate (Figure 3d). The
360 TOC normalized volume of fluorescence for Pf-MBR1 was reduced by 60% (Figure 3b and
361 Figure 3d), while the volume of fluorescence was only reduced by 14% and 10% for P-MBR2
362 and Pw-MBR1, respectively (Figure 3b and Figure 3d). Membrane fouling therefore has a clear
363 effect on fluorophore quantity, via restricting EfOM permeation (Figure 3b). Indeed, more
364 fluorescent compounds are retained, on a per carbon basis, by a fouled membrane. This result
365 shows that the fouling layer on the membrane surface selectively removes compounds rich in
366 functional groups with high electron density, which are more reactive with ROS than other
367 moieties. Pw-MBR1 and P-MBR2 are therefore expected to quench photocatalysis to a greater
368 extent. This assumption is supported by the $SUVA_{254}$ data: values for the Pf-MBR1, Pw-MBR1,
369 and P-MBR2 samples were measured to be 0.8, 2.0, and 2.0 $L \cdot mg^{-1} \cdot m^{-1}$, respectively. Pf-
370 MBR1, having a $SUVA_{254}$ value of 0.8 $L \cdot mg^{-1} \cdot m^{-1}$, is characterized by non-aromatic organic
371 compounds and therefore fewer potential functional groups reactive with ROS. On the
372 contrary, Pw-MBR1 and P-MBR2, with $SUVA_{254}$ values of 2.0 $L \cdot mg^{-1} \cdot m^{-1}$, contain more
373 aromatic compounds, which may preferentially compete with ROS.

374 Control of membrane fouling may provide an opportunity to increase photocatalysis process
375 efficiency by regulating the chemical makeup and concentration of EfOM. Less frequent
376 cleaning events could be ideal, since the fouled membranes provided the highest DOM
377 retention. From the fluorescence volumes, it is expected that TiO_2 photocatalysis would be
378 quenched to a greater extent by Pw-MBR1 and P-MBR2, than by Pf-MBR1.

379 3.3. Inhibition of $\bullet\text{OH}$ by DOM Fractions

380 Segregation of MBR DOM into functional categories allowed for a unique examination of the
381 inhibition potential of these functional classes of compounds. Colloidal, HPO, and TPI fractions
382 were each examined for concentration-dependent inhibitory activity. Control tests confirmed
383 the photocatalytic action of TiO_2 and differentiated the role of ROS from the direct photolysis
384 by UV_{254} light (Figure S3). The action by UV_{254} alone represented the lower bound of $k_{\text{obs},\rho\text{CBA}}$,
385 where $\bullet\text{OH}$ radicals were completely quenched by DOM. Likewise, the case of TiO_2 and ρCBA
386 in pure water served as the upper bound of photocatalytic efficiency, with no interfering
387 quenching agents. The $k_{\text{obs},\rho\text{CBA}}$ values plotted in Figure 4 showed that of the three DOM
388 fractions, colloids exerted the strongest inhibition by far. The corresponding k'_{obs} (s^{-1}) data is
389 shown in Figure S4. The TPI and HPO portions were similar in their effect on $k_{\text{obs},\rho\text{CBA}}$, and
390 exerted mild inhibition at low TOC concentrations. Interestingly, for both TPI and HPO, the
391 $k_{\text{obs},\rho\text{CBA}}$ increased from 7.5 to 10 mgC/L . This increase in photodegradation efficacy was

392 surprising but not unprecedented; it was recently reported that Natural Organic Matter (NOM)
393 actually enhanced the TiO₂-driven photodegradation of carbamazepine, pharmaceutical
394 compound, at specific TiO₂:NOM ratios, by up to 8%.⁷⁶ Favorable NOM-carbamazepine
395 interactions explained the increased effectiveness; these interactions draw the compound
396 closer to the active surface sites of TiO₂, where •OH are present at higher concentrations. The
397 colloidal fraction did not increase the photoactivity at any concentration. Examination of the
398 inhibition profiles of the three DOM fractions in the context of 3DEEM analysis (Figure 1)
399 suggested that the quenching action of the DOM fractions is correlated to higher concentration
400 of colloids, which are characterized by a higher proportion of fluorescence in Region I and
401 Region II (Figure 1a). This observation suggests that despite higher volumes of fluorescence,
402 HPO and TPI are less potent inhibitors of photocatalysis than the colloids. The surface
403 interactions, and therefore inhibition mechanism, of the colloids with the TiO₂ surface could be
404 fundamentally different from that of the HPO and TPI fractions, because the colloidal fraction
405 was not segregated based on surface character, but rather by size only. Control of membrane
406 surface properties and fouling could reduce the colloidal content—much of which consists of
407 high molecular weight molecules that can be preferentially retained—in EfOM and thereby
408 mitigate the quenching of photocatalytic processes by DOM.²³



409

410 Figure 4: ρ CBA degradation rate constants in the presence of 5 mg/L TiO_2 and various
 411 concentrations of colloids, TPI, HPO, and HA are depicted here. The rate constant for ρ CBA
 412 degradation by UVC without TiO_2 is also shown. Ambient temperature was measured at 24
 413 °C.

414

415 3.4. Inhibition of $\bullet\text{OH}$ by EfOM

416 The EfOM of the three MBR permeate samples, as described above, was tested for inhibition
 417 potential of $\bullet\text{OH}$ -mediated ρ CBA degradation. The samples were examined on a TOC basis
 418 to discern changes in inhibition potential caused by qualitative differences in EfOM
 419 composition. A low concentration of TiO_2 , relative to that used in similar studies on
 420 photocatalyst-DOM interactions,^{29, 38, 77, 78} was selected to avoid the effects of EfOM

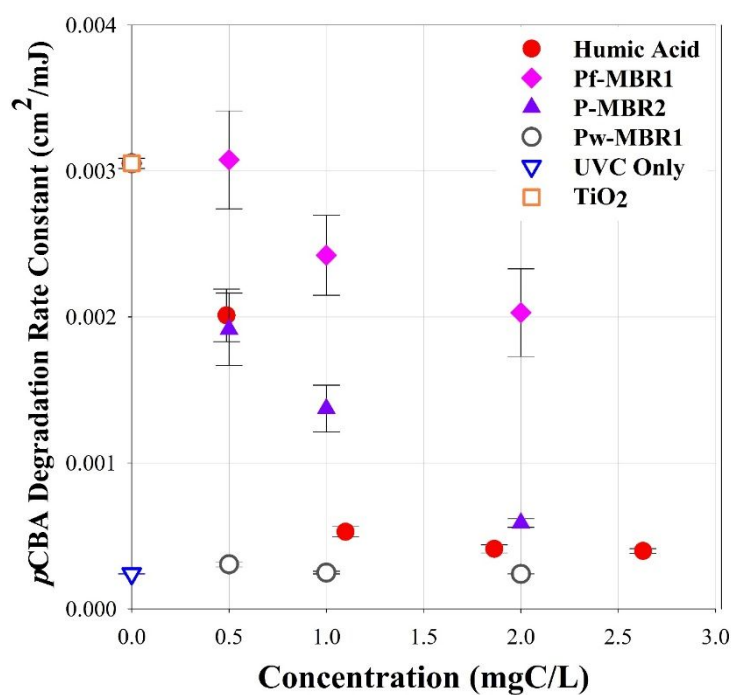
421 transformation by oxidation. Hour-long UVC irradiation experiments with 10 mg/L HA and
422 various concentrations of TiO₂ showed that *p*CBA photodegradation kinetics were linear for
423 the TiO₂ concentration of 5 mg/L. Tests with TiO₂ concentrations of 100 mg/L or higher showed
424 accelerating kinetics and suggested that HA was itself being degraded by •OH radicals so that
425 its inhibition potential changed with time.

426 The inhibition capacities of MBR EfOM samples were evaluated by measuring $k_{\text{obs},p\text{CBA}}$ as a
427 function of individual EfOM sample concentrations. These rates were calculated across
428 concentrations ranging from 0 to 2.3 mgC/L (Figure 5). The corresponding k'_{obs} (1) data is
429 shown in Figure S5. Comparing $k_{\text{obs},p\text{CBA}}$ values for the same TOC content reveals that the
430 state of membrane fouling drove clear distinctions in inhibitory activity of the EfOM. While it
431 was expected that a fouled membrane would reject more DOM than a clean membrane, the
432 inhibition capacity on a per carbon basis was not known. Here, it was observed that EfOM from
433 a fouled membrane system inhibited the photocatalytic process much less than EfOM from a
434 cleaned membrane. At just 0.5 mgC/L, Pw-MBR1 quenched the photocatalytic process
435 completely, while no quenching was observed by Pf-MBR1 EfOM at the same concentration.
436 This result provides evidence that the changes in EfOM composition caused by membrane
437 fouling; the reduction of colloid concentration and total fluorophores is especially beneficial for
438 photocatalytic operation. 3DEEM confirmed that molecules containing fluorescent groups in

439 Regions I and II impact photocatalytic performance more than other compounds. Qualitative
440 changes in DOM retention by the membrane, therefore, impacted the photocatalytic quenching
441 process. Considering these results in the context of the DOM fractions analysis, retention of
442 organic colloids by the fouled membrane was likely enhanced by the formation of a fouling
443 layer.^{3, 22} Inhibition by P-MBR2, sourced from a membrane at the midpoint between chemical
444 cleanings, was between the two extremes of Pw- and Pf-MBR1, with a ~75% reduction in
445 $k_{\text{obs},\rho\text{CBA}}$ at 0.5 mgC/L. Alternatively, it may be possible to choose or modify membrane
446 materials to selectively reject the organic colloidal materials regardless of the fouling state. HA
447 served as a reference material, which represents NOM found in drinking water sources more
448 closely than EfOM, and exhibited stronger quenching than the P-MBR2 case but less inhibition
449 than Pw-MBR1. It is noteworthy that HA inhibits TiO_2 driven photocatalysis to a greater extent
450 than EfOM from a fouled MBR on a carbon basis. This finding contradicts a 'common sense'
451 assumption that could be made based solely on TOC values: that photocatalysis would be
452 more applicable for drinking water applications than for WWTP effluent.

453 The 3DEEM analyses (Figure 3) of the MBR EfOM samples predicted that the fouled
454 membrane would reduce the quantity of fluorescent compounds in the EfOM and therefore
455 lead to less inhibition of photocatalysis. However, for cases of similar fluorescence volumes,
456 as for Pw-MBR1 and P-MBR2 in particular, the use of 3DEEM did not explain differences in

457 inhibitory action. In these cases, other factors, such as the hydrophobic/hydrophilic character
 458 of the EfOM, may have been altered by the membrane fouling but not detected by 3DEEM or
 459 TOC analysis. It is well known that membrane fouling affects rejection of DOM components⁴¹,
 460 ^{43, 79} and that the mechanism of action is not simply size exclusion alone: changes in the
 461 surface characteristics (i.e. charge and hydrophobicity), due to fouling layer formation, are also
 462 important.^{3, 22}



463
 464 Figure 5: ρ CBA degradation rate constants in the presence of various concentrations of HA,
 465 effluents from Pf-MBR1, from Pw-MBR1, and from P-MBR2 with 5 mg/L TiO₂ are depicted
 466 here. The rate constant for pCBA degradation by UVC without TiO₂ is also shown.

467

468 3.5. Inhibitory mechanisms for DOM samples

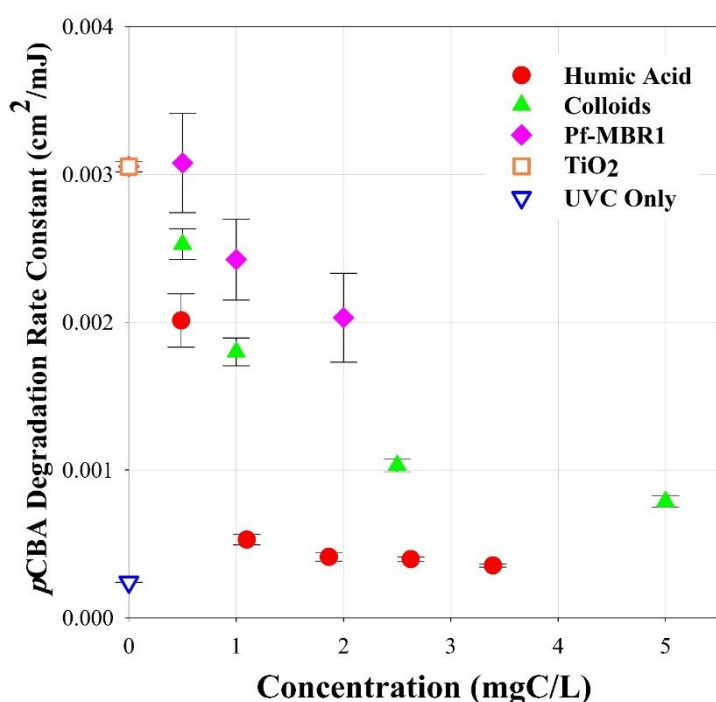
469 Identification of the mechanism of inhibition by DOM on TiO₂ photocatalysis is the key to
470 designing processes to overcome the problem of ROS quenching. Numerous studies have
471 evaluated the adsorption interactions of NOM onto TiO₂, fitting experimental findings to
472 Freundlich⁸⁰ or Langmuir-Hinshelwood^{32, 77, 81} isotherms. Only recently, however, was a model
473 developed that accounted for both bulk- and surface-phase quenching interactions.²⁹ In their
474 work, Brame et al. experimentally validated a model that combined a multi-solute Langmuir
475 model⁸² with bulk phase competitive reaction rates by assuming steady-state ROS
476 concentrations.²⁹ Based on this dual-phase model, the mode of inhibition (bulk or surface
477 reactions) was successfully predicted by analysis of the dependency of k_{obs} on TOC. A linear
478 dependence of k_{obs} on TOC implied that inhibition primarily occurred in the bulk phase and
479 surface interactions were unimportant; alternatively, an exponential decay of k_{obs} with
480 increasing TOC indicated that surface sorption and reactions played a significant role in the
481 inhibitory process.²⁹ Note that the aforementioned report used Suwannee River humic acid as
482 an NOM source, which consists of a wide range of molecules;²⁹ applying Brame's model in
483 experiments with fractionated DOM samples is an important extension of the earlier work
484 allowing for a discriminating analysis of inhibition mechanisms across the DOM spectrum.
485 Here, all experiments were performed with the same probe compound, photocatalyst
486 concentration, and UV₂₅₄ lamp, so normalization of $k_{\text{obs},\rho\text{CBA}}$ was not necessary. The inhibition

487 profile for HA was non-linear and therefore depended on surface interactions, in line with
488 previous reports for TiO₂ inhibition by NOM.^{29, 38, 83, 84} Upon examination of the inhibitory profiles
489 of the MBR effluents, trends for Pf-MBR1 and P-MBR2 were noted to be nearly linear, whereas
490 Pw-MBR1 showed an exponential relationship. These observations suggest that the
491 membrane fouling layer played a critical role by rejecting DOM that adsorbs favorably onto the
492 surface of TiO₂, thereby exerting a strong quenching effect on photocatalytic processes. These
493 observations correlate well with the observed inhibition profiles of the fractionated DOM.

494 As discussed, the colloidal fraction of BSN DOM exerted the strongest inhibitory action of any
495 of the fractions (Figure 4). The $k_{\text{obs},\rho\text{CBA}}$ inhibition profiles of the DOM fractions reveal that the
496 colloids quenched the photocatalytic process via sorption onto the TiO₂ surface and reacting
497 with surface-bound •OH. The HPO and TPI fractions, however, displayed a linear
498 dependence—if the spurious enhancement of $k_{\text{obs},\rho\text{CBA}}$ at the 10 mgC/L mark is neglected—on
499 TOC. The HPO and TPI samples, therefore, primarily reduced $k_{\text{obs},\rho\text{CBA}}$ through bulk phase
500 reactions limited by diffusion and relative reaction rates. Note that these remarks on quenching
501 mechanisms are generalizations: even the fractionated DOM samples contain a wide variety
502 of molecules, each with specific adsorption affinities and reaction rates. Still, results of both
503 fractionation and membrane fouling conditions showed significant changes to inhibitory action
504 of DOM. The inhibitory action of the colloidal fraction was particularly interesting, given the lack

505 of inhibitory action by effluent from the fouled membrane. These observations taken together
506 in Figure 6 (data replotted from Figures 4 and 5) suggest that fouled membranes reject key
507 organic colloids that would otherwise adsorb strongly to TiO_2 surfaces and greatly reduce
508 photodegradation rates. The corresponding k'_{obs} (s^{-1}) data is shown in Figure S6. The
509 prospective utility of a membrane for pretreatment is clearly demonstrated by these results: if
510 a membrane can be selected or optimized to reject problematic colloids, photocatalysis may
511 indeed be effective for disinfection of MBR effluent.

512



513

514 Figure 6: $k'_{\text{obs}, \rho_{\text{CBA}}}$ inhibition profiles of HA, Pf-MBR1, and the colloidal fraction. Data from
515 Figures 3 and 4 are used here.

516

517 4. Conclusions

518 The challenge of unwanted ROS-DOM reactions has long plagued photocatalysis, particularly
519 for applications dealing with high TOC concentrations such as in a typical MBR effluent.
520 3DEEM can be used to predict the inhibitory effects of DOM composition, and the experiments
521 shed new light on the quenching of photocatalysts by DOM. First, the total fluorescence volume
522 correlated well with the extent of photocatalytic inhibition on a carbon basis, further the DOM
523 fractionation demonstrated that the colloidal fraction of DOM exerted stronger quenching
524 action than HPO and TPI. The membrane fouling status showed that fouled membrane showed
525 very little inhibitory action compared to permeate from clean and moderately fouled
526 membranes. In fact, DOM from fouled membrane appeared to quench $\bullet\text{OH}$ primarily via bulk-
527 phase scavenging, whereas DOM from a clean membrane showed an inhibition profile
528 consistent with surface-phase reactions,²⁸ suggesting that the membrane fouling layer rejected
529 materials that would otherwise adsorb strongly to the TiO_2 surface. To enhance photocatalysis
530 efficiency, it might be possible to select a membrane with a “built-in” selectivity similar to that
531 of the fouled membrane in order to remove the problematic colloidal fraction. Analysis of the
532 inhibition profiles of the EfOM described here suggests that for the operation of a PMR a trade-
533 off can be made between the operational pressure and the photocatalytic efficiency; by
534 reducing the (chemical) cleaning frequency and thereby maintaining a minimal level of fouling,

535 inhibition of photocatalysis by organic colloidal inhibitors would be mitigated at a cost of higher
536 trans-membrane pressures. Further, the surface coverage of TiO_2 on PMRs can be tuned to
537 optimize photocatalyst surface area⁸⁵ and may not be limited to the DOM: TiO_2 ratios explored
538 here.

539 Further research on the fundamental surface interactions between these organic colloidal
540 materials and photocatalyst or membrane surfaces should be pursued in order to develop
541 mitigation strategies for DOM-related ROS inhibition. Specifically, the assessment of the
542 potential effects of the hydrophilic fraction and dissolved ions (i.e., multivalent cations and
543 halides), which were not retained by the fractionation processes, should be examined. The
544 results of the present study may be applicable to the use of photocatalytic materials in systems
545 containing other DOM sources, therefore additional investigations on systems such as potable
546 water supplies or industrial waste streams would be timely and important.

547

548 **5. Acknowledgements**

549 This material is based upon work supported in part by the Louisiana Board of Regents
550 Research Competitiveness Subprogram under grant LEQSF(2017-20)-RD-A-06 and in part by
551 the National Science Foundation Partnerships for International Research and Education
552 program under Grant IIA-1243433. The authors would like to thank the operators at the La

553 Grande Motte wastewater treatment plant for providing access to their facility and assistance
 554 with collecting wastewater samples for analysis.

555

556 6. References

- 557 1. R. L. Droste, *Theory and Practice of Water and Wastewater Treatment*, John Wiley & Sons,
 558 Inc., New York, 1997.
- 559 2. L. B. Franklin, *Wastewater Engineering: Treatment, Disposal and Reuse*, McGraw Hill, Inc.,
 560 New York, 1991.
- 561 3. O. T. Iorhemen, R. A. Hamza and J. H. Tay, Membrane Bioreactor (MBR) Technology for
 562 Wastewater Treatment and Reclamation: Membrane Fouling, *Membranes*, 2016, **6**, 1-29.
- 563 4. D. S. Francy, E. A. Stelzer, R. N. Bushon, A. M. G. Brady, A. G. Williston, K. R. Riddell, M.
 564 A. Borchardt, S. K. Spencer and T. M. Gellner, Comparative effectiveness of membrane
 565 bioreactors, conventional secondary treatment, and chlorine and UV disinfection to remove
 566 microorganisms from municipal wastewaters, *Water Res.*, 2012, **46**, 4164-4178.
- 567 5. E. O'Brien, M. Munir, T. Marsh, M. Heran, G. Lesage, V. V. Tarabara and I. Xagorarakis,
 568 Diversity of DNA viruses in effluents of membrane bioreactors in Traverse City, MI (USA) and
 569 La Grande Motte (France), *Water Res.*, 2017, **111**, 338-345.
- 570 6. Y. P. Zhang and J. L. Zhou, Occurrence and removal of endocrine disrupting chemicals in
 571 wastewater, *Chemosphere*, 2008, **73**, 848-853.
- 572 7. Y. L. Luo, W. S. Guo, H. H. Ngo, L. D. Nghiem, F. I. Hai, J. Zhang, S. Liang and X. C. C.
 573 Wang, A review on the occurrence of micropollutants in the aquatic environment and their fate
 574 and removal during wastewater treatment, *Sci. Total Environ.*, 2014, **473**, 619-641.
- 575 8. M. Munir, K. Wong and I. Xagorarakis, Release of antibiotic resistant bacteria and genes in the
 576 effluent and biosolids of five wastewater utilities in Michigan, *Water Res.*, 2011, **45**, 681-693.
- 577 9. I. Kim, N. Yamashita and H. Tanaka, Performance of UV and UV/H₂O₂ processes for the
 578 removal of pharmaceuticals detected in secondary effluent of a sewage treatment plant in Japan,
 579 *J. Hazard. Mater.*, 2009, **166**, 1134-1140.
- 580 10. M. Klavarioti, D. Mantzavinos and D. Kassinos, Removal of residual pharmaceuticals from
 581 aqueous systems by advanced oxidation processes, *Environ. Int.*, 2009, **35**, 402-417.
- 582 11. L. Yang, L. E. Yu and M. B. Ray, Degradation of paracetamol in aqueous solutions by TiO₂
 583 photocatalysis, *Water Res.*, 2008, **42**, 3480-3488.
- 584 12. Y. J. Meng, Y. Wang, Q. Han, N. Xue, Y. Y. Sun, B. Y. Gao and Q. L. Li, Trihalomethane
 585 (THM) formation from synergic disinfection of biologically treated municipal wastewater:
 586 Effect of ultraviolet (UV) irradiation and titanium dioxide photocatalysis on dissolve organic
 587 matter fractions, *Chem. Eng. J.*, 2016, **303**, 252-260.
- 588 13. J. C. Crittenden, R. Rhodes Trussell and D. W. Hand, *MWH's Water Treatment: Principles and
 589 Design*, John Wiley & Sons, Inc., Hoboken, New Jersey, 2012.
- 590 14. W. A. M. Hijnen, E. F. Beerendonk and G. J. Medema, Inactivation credit of UV radiation for
 591 viruses, bacteria and protozoan (oo)cysts in water: A review, *Water Res.*, 2006, **40**, 3-22.
- 592 15. M. Cho, H. M. Chung, W. Y. Choi and J. Y. Yoon, Different inactivation Behaviors of MS-2
 593 phage and Escherichia coli in TiO₂ photocatalytic disinfection, *Appl. Environ. Microbiol.*, 2005,
 594 **71**, 270-275.
- 595 16. S. D. Snow, K. Park and J.-H. Kim, Cationic Fullerene Aggregates with Unprecedented Virus
 596 Photoinactivation Efficiencies in Water, *Environ. Sci. Tech. Let.*, 2014, **1**, 290-294.

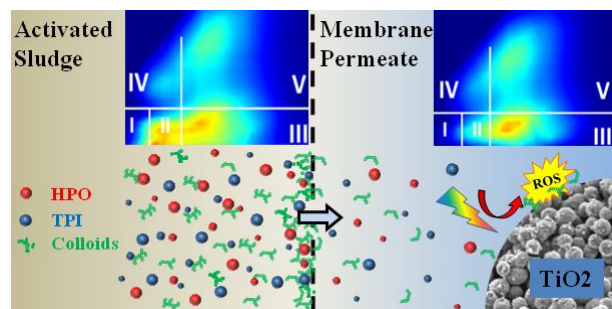
- 597 17. S. Malato, P. Fernandez-Ibanez, M. I. Maldonado, J. Blanco and W. Gernjak, Decontamination
598 and disinfection of water by solar photocatalysis: Recent overview and trends, *Catal. Today*,
599 2009, **147**, 1-59.
- 600 18. M. Cho, H. Chung, W. Choi and J. Yoon, Linear correlation between inactivation of E. coli and
601 OH radical concentration in TiO₂ photocatalytic disinfection, *Water Res.*, 2004, **38**, 1069-1077.
- 602 19. J. A. Grant and R. Hofmann, A comparative study of the hydroxyl radical scavenging capacity
603 of activated sludge and membrane bioreactor wastewater effluents, *Water Sci. Technol.*, 2016,
604 **73**, 2067-2073.
- 605 20. S. Tang, Z. Wang, Z. Wu and Q. Zhou, Role of dissolved organic matters (DOM) in membrane
606 fouling of membrane bioreactors for municipal wastewater treatment, *J. Hazard. Mater.*, 2010,
607 **178**, 377-384.
- 608 21. K. Chon, K. Lee, I.-S. Kim and A. Jang, Performance assessment of a submerged membrane
609 bioreactor using a novel microbial consortium, *Bioresour. Technol.*, 2016, **210**, 2-10.
- 610 22. C. Jarusutthirak, G. Amy and J.-P. Croué, Fouling characteristics of wastewater effluent organic
611 matter (EfOM) isolates on NF and UF membranes, *Desalination*, 2002, **145**, 247-255.
- 612 23. C. Jacquin, B. Teychene, L. Lemeé, G. Lesage and M. Heran, Characteristics and fouling
613 behaviors of Dissolved Organic Matter fractions in a full-scale submerged membrane bioreactor
614 for municipal wastewater treatment, *Biochem. Eng. J.*, 2018, **132**, 169-181.
- 615 24. P. Wang, Z. W. Wang, Z. C. Wu and S. H. Mai, Fouling behaviours of two membranes in a
616 submerged membrane bioreactor for municipal wastewater treatment, *J. Membr. Sci.*, 2011,
617 **382**, 60-69.
- 618 25. C. Kunacheva, C. Le, Y. N. A. Soh and D. C. Stuckey, Chemical Characterization of Low
619 Molecular Weight Soluble Microbial Products in an Anaerobic Membrane Bioreactor, *Environ.*
620 *Sci. Technol.*, 2017, **51**, 2254-2261.
- 621 26. J. Y. Sun, K. Xiao, Y. H. Mo, P. Liang, Y. X. Shen, N. W. Zhu and X. Huang, Seasonal
622 characteristics of supernatant organics and its effect on membrane fouling in a full-scale
623 membrane bioreactor, *J. Membr. Sci.*, 2014, **453**, 168-174.
- 624 27. K. Xiao, Y. X. Shen, S. Liang, P. Liang, X. M. Wang and X. Huang, A systematic analysis of
625 fouling evolution and irreversibility behaviors of MBR supernatant hydrophilic/hydrophobic
626 fractions during microfiltration, *J. Membr. Sci.*, 2014, **467**, 206-216.
- 627 28. S. Giannakis, S. Liu, A. Carratalà, S. Rtimi, M. Talebi Amiri, M. Bensimon and C. Pulgarin,
628 Iron oxide-mediated semiconductor photocatalysis vs. heterogeneous photo-Fenton treatment
629 of viruses in wastewater. Impact of the oxide particle size, *J. Hazard. Mater.*, 2017, **339**, 223-
630 231.
- 631 29. J. Brame, M. Long, Q. Li and P. Alvarez, Inhibitory effect of natural organic matter or other
632 background constituents on photocatalytic advanced oxidation processes: Mechanistic model
633 development and validation, *Water Res.*, 2015, **84**, 362-371.
- 634 30. G. V. Buxton, C. L. Greenstock, W. P. Helman and A. B. Ross, Critical review of rate constants
635 for reactions of hydrated electrons, hydrogen atoms and hydroxyl radicals (.OH/.O-) in aqueous
636 solution, *J. Phys. Chem. Ref. Data*, 1988, **17**, 513-886.
- 637 31. S. Kim and W. Choi, Kinetics and mechanisms of photocatalytic degradation of (CH₃)_nNH₄ⁿ⁺
638 (0 ≤ n ≤ 4) in TiO₂ suspension: The role of OH radicals, *Environ. Sci. Technol.*, 2002, **36**,
639 2019-2025.
- 640 32. R. Enriquez and P. Pichat, Interactions of Humic Acid, Quinoline, and TiO₂ in Water in
641 Relation to Quinoline Photocatalytic Removal, *Langmuir*, 2001, **17**, 6132-6137.
- 642 33. C. Kunacheva, Y. N. A. Soh, A. P. Trzcinski and D. C. Stuckey, Soluble microbial products
643 (SMPs) in the effluent from a submerged anaerobic membrane bioreactor (SAMBR) under
644 different HRTs and transient loading conditions, *Chem. Eng. J.*, 2017, **311**, 72-81.
- 645 34. Y. Yang, J. J. Pignatello, J. Ma and W. A. Mitch, Effect of matrix components on UV/H₂O₂
646 and UV/S₂O₈²⁻ advanced oxidation processes for trace organic degradation in reverse osmosis
647 brines from municipal wastewater reuse facilities, *Water Res.*, 2016, **89**, 192-200.
- 648 35. F. L. Rosario-Ortiz, E. C. Wert and S. A. Snyder, Evaluation of UV/H₂O₂ treatment for the
649 oxidation of pharmaceuticals in wastewater, *Water Res.*, 2010, **44**, 1440-1448.
- 650 36. N. Senesi, Binding mechanisms of pesticides to soil humic substances, *Sci. Total Environ.*,
651 1992, **123-124**, 63-76.

- 652 37. J. D. Ritchie and E. M. Perdue, Proton-binding study of standard and reference fulvic acids,
653 humic acids, and natural organic matter, *Geochim. Cosmochim. Acta*, 2003, **67**, 85-96.
- 654 38. J. Brame, M. C. Long, Q. L. Li and P. Alvarez, Trading oxidation power for efficiency:
655 Differential inhibition of photo-generated hydroxyl radicals versus singlet oxygen, *Water Res.*,
656 2014, **60**, 259-266.
- 657 39. P. R. Ogilby, Singlet oxygen: there is indeed something new under the sun, *Chem. Soc. Rev.*,
658 2010, **39**, 3181-3209.
- 659 40. Z. X. Cai and M. M. Benjamin, NOM Fractionation and Fouling of Low-Pressure Membranes
660 in Microgranular Adsorptive Filtration, *Environ. Sci. Technol.*, 2011, **45**, 8935-8940.
- 661 41. L. Fan, J. L. Harris, F. A. Roddick and N. A. Booker, Influence of the characteristics of natural
662 organic matter on the fouling of microfiltration membranes, *Water Res.*, 2001, **35**, 4455-4463.
- 663 42. E. Filloux, H. Gallard and J.-P. Croue, Identification of effluent organic matter fractions
664 responsible for low-pressure membrane fouling, *Water Res.*, 2012, **46**, 5531-5540.
- 665 43. R. K. Henderson, N. Subhi, A. Antony, S. J. Khan, K. R. Murphy, G. L. Leslie, V. Chen, R. M.
666 Stuetz and P. Le-Clech, Evaluation of effluent organic matter fouling in ultrafiltration treatment
667 using advanced organic characterisation techniques, *J. Membr. Sci.*, 2011, **382**, 50-59.
- 668 44. H. K. Shon, S. Vigneswaran, I. S. Kim, J. Cho and H. H. Ngo, Fouling of ultrafiltration
669 membrane by effluent organic matter: A detailed characterization using different organic
670 fractions in wastewater, *J. Membr. Sci.*, 2006, **278**, 232-238.
- 671 45. P. Le-Clech, V. Chen and T. A. G. Fane, Fouling in membrane bioreactors used in wastewater
672 treatment, *J. Membr. Sci.*, 2006, **284**, 17-53.
- 673 46. F. L. Wang and V. V. Tarabara, Pore blocking mechanisms during early stages of membrane
674 fouling by colloids, *J. Colloid Interface Sci.*, 2008, **328**, 464-469.
- 675 47. Q. L. Li and M. Elimelech, Organic fouling and chemical cleaning of nanofiltration membranes:
676 Measurements and mechanisms, *Environ. Sci. Technol.*, 2004, **38**, 4683-4693.
- 677 48. M. Aslam, A. Charfi, G. Lesage, M. Heran and J. Kim, Membrane bioreactors for wastewater
678 treatment: A review of mechanical cleaning by scouring agents to control membrane fouling,
679 *Chem. Eng. J.*, 2017, **307**, 897-913.
- 680 49. C. S. Uyguner-Demirel, N. C. Birben and M. Bekbolet, Elucidation of background organic
681 matter matrix effect on photocatalytic treatment of contaminants using TiO₂: A review, *Catal.*
682 *Today*, 2017, **284**, 202-214.
- 683 50. P. Mwaanga, E. R. Carraway and M. A. Schlautman, Preferential sorption of some natural
684 organic matter fractions to titanium dioxide nanoparticles: influence of pH and ionic strength,
685 *Environ. Monit. Assess.*, 2014, **186**, 8833-8844.
- 686 51. E. M. Carstea, J. Bridgeman, A. Baker and D. M. Reynolds, Fluorescence spectroscopy for
687 wastewater monitoring: A review, *Water Res.*, 2016, **95**, 205-219.
- 688 52. R. K. Henderson, A. Baker, K. R. Murphy, A. Hambly, R. M. Stuetz and S. J. Khan,
689 Fluorescence as a potential monitoring tool for recycled water systems: A review, *Water Res.*,
690 2009, **43**, 863-881.
- 691 53. C. Jacquin, G. Lesage, J. Traber, W. Pronk and M. Heran, Three-dimensional excitation and
692 emission matrix fluorescence (3DEEM) for quick and pseudo-quantitative determination of
693 protein- and humic-like substances in full-scale membrane bioreactor (MBR), *Water Res.*, 2017,
694 **118**, 82-92.
- 695 54. W. Chen, P. Westerhoff, J. A. Leenheer and K. Booksh, Fluorescence Excitation–Emission
696 Matrix Regional Integration to Quantify Spectra for Dissolved Organic Matter, *Environ. Sci.*
697 *Technol.*, 2003, **37**, 5701-5710.
- 698 55. D. D. Phong and J. Hur, Non-catalytic and catalytic degradation of effluent dissolved organic
699 matter under UVA-and UVC-irradiation tracked by advanced spectroscopic tools, *Water Res.*,
700 2016, **105**, 199-208.
- 701 56. R. X. Hao, H. Q. Ren, J. B. Li, Z. Z. Ma, H. W. Wan, X. Y. Zheng and S. Y. Cheng, Use of
702 three-dimensional excitation and emission matrix fluorescence spectroscopy for predicting the
703 disinfection by-product formation potential of reclaimed water, *Water Res.*, 2012, **46**, 5765-
704 5776.

- 705 57. B. Guo, S. D. Snow, B. J. Starr, I. Xagorarakis and V. V. Tarabara, Photocatalytic inactivation
706 of human adenovirus 40: Effect of dissolved organic matter and prefiltration, *Sep. Purif.*
707 *Technol.*, 2018, **193**, 193-201.
- 708 58. S. Mozia, Photocatalytic membrane reactors (PMRs) in water and wastewater treatment. A
709 review, *Sep. Purif. Technol.*, 2010, **73**, 71-91.
- 710 59. X. Zheng, Z. P. Shen, L. Shi, R. Cheng and D. H. Yuan, Photocatalytic Membrane Reactors
711 (PMRs) in Water Treatment: Configurations and Influencing Factors, *Catalysts*, 2017, **7**, 30.
- 712 60. B. Pernet-coudrier, L. Clouzot, G. Varrault, M.-H. Tusseau-vuillemin, A. Verger and J.-M.
713 Mouchel, Dissolved organic matter from treated effluent of a major wastewater treatment plant:
714 Characterization and influence on copper toxicity, *Chemosphere*, 2008, **73**, 593-599.
- 715 61. D. Violleau, H. Essis-Tome, H. Habarou, J. P. Croué and M. Pontié, Fouling studies of a
716 polyamide nanofiltration membrane by selected natural organic matter: an analytical approach,
717 *Desalination*, 2005, **173**, 223-238.
- 718 62. X. Zheng, M. T. Khan and J.-P. Croué, Contribution of effluent organic matter (EfOM) to
719 ultrafiltration (UF) membrane fouling: Isolation, characterization, and fouling effect of EfOM
720 fractions, *Water Res.*, 2014, **65**, 414-424.
- 721 63. G. R. Aiken, D. M. McKnight, K. A. Thorn and E. M. Thurman, Isolation of hydrophilic organic
722 acids from water using nonionic macroporous resins, *Org. Geochem.*, 1992, **18**, 567-573.
- 723 64. J. A. Leenheer, Systematic Approaches to Comprehensive Analyses of Natural Organic Matter,
724 *Ann. Environ. Sci.*, 2009, **3**.
- 725 65. J. L. Weishaar, G. R. Aiken, B. A. Bergamaschi, M. S. Fram, R. Fujii and K. Mopper, Evaluation
726 of Specific Ultraviolet Absorbance as an Indicator of the Chemical Composition and Reactivity
727 of Dissolved Organic Carbon, *Environ. Sci. Technol.*, 2003, **37**, 4702-4708.
- 728 66. C. Goletz, M. Wagner, A. Grübel, W. Schmidt, N. Korf and P. Werner, Standardization of
729 fluorescence excitation–emission-matrices in aquatic milieu, *Talanta*, 2011, **85**, 650-656.
- 730 67. M. Cho, H. Chung, W. Choi and J. Yoon, Linear correlation between inactivation of *E. coli* and
731 OH radical concentration in TiO₂ photocatalytic disinfection, *Water Res.*, 2004, **38**, 1069-1077.
- 732 68. J. R. Bolton and K. G. Linden, Standardization of methods for fluence (UV dose) determination
733 in bench-scale UV experiments, *ASCE J. Environ. Eng.*, 2003, **129**, 209-215.
- 734 69. M. L. Quaranta, M. D. Mendes and A. A. MacKay, Similarities in effluent organic matter
735 characteristics from Connecticut wastewater treatment plants, *Water Res.*, 2012, **46**, 284-294.
- 736 70. T. Masuda, S. Nakano and M. Kondo, Rate Constants for the Reactions of OH Radicals with
737 the Enzyme Proteins as Determined by the p-Nitrosodimethylaniline Method, *Journal of*
738 *Radiation Research*, 1973, **14**, 339-345.
- 739 71. C. L. Hawkins and M. J. Davies, Generation and propagation of radical reactions on proteins,
740 *Biochim. Biophys. Acta*, 2001, **1504**, 196-219.
- 741 72. Y. Pi, J. Schumacher and M. Jekel, The Use of para-Chlorobenzoic Acid (pCBA) as an
742 Ozone/Hydroxyl Radical Probe Compound, *Ozone: Science & Engineering*, 2005, **27**, 431-436.
- 743 73. I. Michael-Kordatou, C. Michael, X. Duan, X. He, D. D. Dionysiou, M. A. Mills and D. Fatta-
744 Kassinos, Dissolved effluent organic matter: Characteristics and potential implications in
745 wastewater treatment and reuse applications, *Water Res.*, 2015, **77**, 213-248.
- 746 74. A. Matilainen, E. T. Gjessing, T. Lahtinen, L. Hed, A. Bhatnagar and M. Sillanpaa, An overview
747 of the methods used in the characterisation of natural organic matter (NOM) in relation to
748 drinking water treatment, *Chemosphere*, 2011, **83**, 1431-1442.
- 749 75. J. K. Edzwald and J. E. Tobiasson, Enhanced coagulation: Us requirements and a broader view,
750 *Water Sci. Technol.*, 1999, **40**, 63-70.
- 751 76. M. Drosos, M. J. Ren and F. H. Frimmel, The effect of NOM to TiO₂: interactions and
752 photocatalytic behavior, *Appl. Catal. B-Environ.*, 2015, **165**, 328-334.
- 753 77. Y. Sun and J. J. Pignatello, Evidence for a surface dual hole-radical mechanism in the titanium
754 dioxide photocatalytic oxidation of 2,4-D, *Environ. Sci. Technol.*, 1995, **29**, 2065-2072.
- 755 78. X. Huang, M. Leal and Q. Li, Degradation of natural organic matter by TiO₂ photocatalytic
756 oxidation and its effect on fouling of low-pressure membranes, *Water Res.*, 2008, **42**, 1142-
757 1150.
- 758 79. E. Bouhabila, R. Ben Aim and H. Buisson, Fouling characterisation in membrane bioreactors,
759 *Sep. Purif. Technol.*, 2001, **22-3**, 123-132.

- 760 80. S. L. Gora and S. A. Andrews, Adsorption of natural organic matter and disinfection byproduct
761 precursors from surface water onto TiO₂ nanoparticles: pH effects, isotherm modelling and
762 implications for using TiO₂ for drinking water treatment, *Chemosphere*, 2017, **174**, 363-370.
- 763 81. J. F. Budarz, A. Turolla, A. F. Piasecki, J. Y. Bottero, M. Antonelli and M. R. Wiesner, Influence
764 of Aqueous Inorganic Anions on the Reactivity of Nanoparticles in TiO₂ Photocatalysis,
765 *Langmuir*, 2017, **33**, 2770-2779.
- 766 82. C. S. Turchi and D. F. Ollis, Photocatalytic degradation of organic water contaminants:
767 Mechanisms involving hydroxyl radical attack, *J. Catal.*, 1990, **122**, 178-192.
- 768 83. T. E. Doll and F. H. Frimmel, Photocatalytic degradation of carbamazepine, clofibric acid and
769 iomeprol with P25 and Hombikat UV100 in the presence of natural organic matter (NOM) and
770 other organic water constituents, *Water Res.*, 2005, **39**, 403-411.
- 771 84. M. Long, J. Brame, F. Qin, J. Bao, Q. Li and P. J. Alvarez, Phosphate Changes Effect of Humic
772 Acids on TiO₂ Photocatalysis: From Inhibition to Mitigation of Electron-Hole Recombination,
773 *Environ. Sci. Technol.*, 2017, **51**, 514-521.
- 774 85. B. J. Starr, V. V. Tarabara, M. Herrera-Robledo, M. Zhou, S. Roualdès and A. Ayrál, Coating
775 porous membranes with a photocatalyst: Comparison of LbL self-assembly and plasma-
776 enhanced CVD techniques, *J. Membr. Sci.*, 2016, **514**, 340-349.

777



Organic matter from a membrane bioreactor is fractionated and characterized in novel ways to understand component-specific inhibition of photooxidation reactions.